Rock Physics Modeling of Silicious and Carbonate Facies: Conceptual AVO Models Applied to Reservoirs Around the Globe

Alan Mur[1] and Lev Vernik[1]

[1] *Ikon Science Americas*

ABSTRACT

We assembled and expanded a database of siliciclastic log data and published laboratory measurements on dry carbonate samples to demonstrate micromechanics-based methods of rock physics modeling of carbonate rocks coming from diverse depositional and diagenetic environments. By focusing on the effects of mineralogy, porosity, pore shapes, and effective stress on elastic properties of limestones and dolomites in a wide 2-45% porosity range, we show that the Vernik-Kachanov rock physics model (RPM), previously developed for siliciclastics, can be successfully used in seismic reservoir characterization of carbonates worldwide. This rock physics model adheres to the strict micromechanics principles (effective field theory) and allows us to account for realistic pore shapes and separate them from the effects of cracks. Because of the very diverse pore geometries typically observed in carbonates, we use thin section image analysis yielding pore perimeters and areas, which allow us to constrain the pore stiffness represented by the pore shape factors. We subdivide, wherever feasible, the database into textural and mineralogical facies and analyze differences and similarities between them in terms of elastic modeling, which may be utilized in AVO inversion-based reservoir characterization efforts worldwide.

KEY WORDS: Rock Physics, Carbonates, Sands, Shales, AVO Modeling

INTRODUCTION

A key difference between carbonate and siliciclastic rock physics modeling and feasibility for prospect de-risking is in (1) the relatively greater stiffness implied by the carbonate mineralogy, (2) the more advanced diagenetic cementation, and (3) the more complex pore microstructure (Rafavich et al., 1984; Eberly et al., 2003; Baechle et al., 2008). Our ability to account for, let alone model, these effects is still quite limited. Mur and Vernik (2019) discussed calibration techniques and implications of the contact theory and ellipsoidal inclusion-based models in siliciclastic sands and shales and concluded that the use of any "effective pore geometry" (e.g., ellipsoid aspect ratio) often leads to confusion and/or misinterpretation when actual data on pore geometries are available (Vernik and Kachanov, 2010). Mur and Vernik (2020) extended the Vernik and Kachanov (2010) model to carbonates and showed the model effectively handles tasks for carbonate rock physics modeling and feasibility for prospect de-risking.

We use image analysis workflow (Mur et al., 2011) to constrain pore shape factor and then use the calibrated models for scenario testing at key Asia-Pacific reservoirs, further establishing the readiness of the model for log repair and forward modeling for AVO inversion feasibility and post inversion reservoir characterization.

DATABASE

In Mur and Vernik (2019) we compiled and conditioned a database of siliciclastic sand and shale elastic and petrophysical log data with a wide porosity range (8% to 35%). In this database, mechanical compaction and chemical diagenetic effects are well represented across global Jurassic to Miocene age reservoirs. The carbonate database we compiled is sourced from (Rafavich et al., 1984; Baechle et al., 2008; Fabricius et al., 2010; Vasquez et al., 2019). The main criterium for the database selection was controlled laboratory experiments on dry carbonate rocks under the effective stress range from 20-40 MPa to minimize inaccuracy in ultrasonic travel time picking (i.e. we avoid uncertainties from poor core jacket coupling at lower stresses). The database incorporates a wide variety of carbonate depositional environments and diagenetic alteration patterns affecting their porosity and pore geometry discussed in multiple publications (Dunham, 1962; Cantrell and Hagerty, 1999). Table 1 shows the fluid and mineral elastic properties utilized for both rock physics and 1D AVO synthetic modeling.

In order to demonstrate a grounded approach for evaluation of the numerical pore shape factors affecting elastic properties of solids with inclusions of complex shape, we undertook a modified image analysis workflow on some of the typical pore types documented by Cantrell and Hagerty (1999) and Scholle et al (2003).

ROCK PHYSICS MODEL

The Vernik-Kachanov (VK) model is selected here. Originally designed for sandstones (Vernik and Kachanov, 2010; Vernik, 2016) and extended to carbonates (Mur and Vernik (2020)), the VK RPM has the following advantages: (1) it is based on the rigorous theoretical principles with some necessary empirical plug-ins to handle the complexity observed in rocks as compared to any composite materials, (2) it is relatively simple, but does tend to account for the actually observed pore geometries and microcrack densities with the latter allowing for the stress sensitivity of the model, (3) the RPM can be extended into the domain of less consolidated rocks by identifying the critical porosity and the consolidation porosity, and (4) the RPM is formulated for dry rock frame and therefore can be easily transformed using the Gassmann equation to model fluid saturation and compressibility. The RPM is based on the non-interaction approximation method (Kachanov, 1993) combined with the Mori-Tanaka-Benveniste (effective field theory) approach placing both pores and cracks into the average effective stress in the solid matrix of the material.

Pore geometries are represented by pore shape factors, p (for bulk modulus calculations) and q (for shear modulus calculations), which are themselves modeled by their departure from sphericity in the mineral matrix. The pore shape factors in carbonate rocks are greater than in sandstones because of the greater Poisson's ratio of the mineral matrix. Moreover, the shape factors for spherical pores are quite different, namely $p_{sphere} > q_{sphere}$, which necessitates separate

computation of p and q as a function of porosity: $p = p_{sphere} + b_p \phi$, $q = q_{sphere} + b_q \phi$. Another model parameter in this RPM is the normalized compliance due to cracks (microcracks), $A(\nu_m)\eta_0 \exp(-d\sigma)$ for the bulk and $B(\nu_m)\eta_0 \exp(-d\sigma)$ for the shear effective moduli. In these equations η_0 is the crack density at zero stress, σ is the effective stress, and d is a constant which can be set to approximately 0.07 to best account for the laboratory data on P-and S-wave velocity variation with stress in both sandstones and carbonates. The zero-stress crack density in the model is also empirically computed as a function of porosity: $\eta_0 = c + 2.0\phi$, where $c = 0.2$ (for moderate level of stress sensitivity). The matrix coefficients $A(\nu_m)$ and $B(\nu_m)$ are known functions of the matrix Poisson's ratio (Kachanov, 1993).

ROCK PHYSICS MODEL CALIBRATION

Figures 2 and 3 cross plot acoustic impedance (*AI*) vs. porosity (shear impedance vs. porosity is also used to aid calibration, but not shown) for the entire carbonate and siliciclastic datasets, respectively. Table 2 lists the VK RPM input parameters used to calibrate the models, keeping the effective stress constant at 30 MPa for carbonates and 25 MPa for sands. We tentatively assigned the same critical and consolidation porosity values to the entire carbonate core data set ($\phi_c = 0.62$ and $\phi_{con} = 0.3$) and the entire log sandstone data set ($\phi_c = 0.38$ and $\phi_{con} = 0.26$). The exponents m and n, which define the shape of the model line in the poorly consolidated domain, i.e., at $\phi_{con} > 0.3$, are also set constant at 2.2 and 1.8 for carbonates and 2 and 2.05 for sands, respectively.

The pore shape factors p and q were quantified using image analysis that yields both the perimeter and the area of an individual pore. We use the approach suggested by Zimmerman (Jaeger et al., 2007) whereby the geometry factor (GF) in 2D is computed first as

$$GF = \frac{\Pi^2}{4\pi A}, \qquad (1)$$

where Π is the perimeter and A is the area of the pore ($GF = 1.0$ for a sphere). This factor represents departure from circularity (unity). The greater the GF, the greater are the final pore shape factors $p = p_{sphere}*GF$ and $q = q_{sphere}*GF$, and the greater is the pore volume compressibility.

As conceptually shown in Figure 1, the scaling coefficients that correspond to quite isometric moldic pores types average 1.5 ± 0.3 in the image, so that their median pore shape factors are $p = 3.8 \pm 0.8$ and $q = 2.9 \pm 0.6$. The average GF is higher in the tight, microporous mudstone (2.7 ± 1.3) resulting in softer pore shapes with $p = 6.8 \pm 3.3$ and $q = 5.2 \pm 2.5$. However, in general just like in sandstones, the pore shape factors in carbonates seem to be positively correlated to porosity, which tends to amplify the porosity-controlled softening of the rocks. In practice, a small perturbation of $+1.2$ is added to the porosity dependent pore shape factor formulation to account for slightly softer pore shapes than those of spherical pores (as $\phi \rightarrow 0$).

p mean	q mean	p mean	q mean	p mean	q mean
3.8	2.9	6.8	5.2	6.3	4.8

Leached ooids from a grainstone
Scholle et al (2003)

Micropore casts - Arab carbonates
Cantrell (1999)

Danish N. Sea Chalk
Scholle et al (2003)

Figure 1 Key carbonate pore structures and calculated pore shape factors

Figure 2 shows the impressive match that the VK model provides for clean limestones, with all their textural facies (grainstones, packstones, wackestones, and mudstones) falling closely along the RPM line. The subset of dolomites in our database is not adequately characterized in terms of their texture and mineralogy; therefore, this subset is shown in one color on all figures, where applicable. The same applies to the subset of Mg-clay-contaminated limestones from Vasquez et al. (2019) as sampled presalt formations offshore Brazil. This subset is quite diverse in terms of the Mg-clay content varying from 0.02-0.2, and we model it using a Reuss mixture of 88% calcite and 12% clay (light blue dotted line on Figure 1).
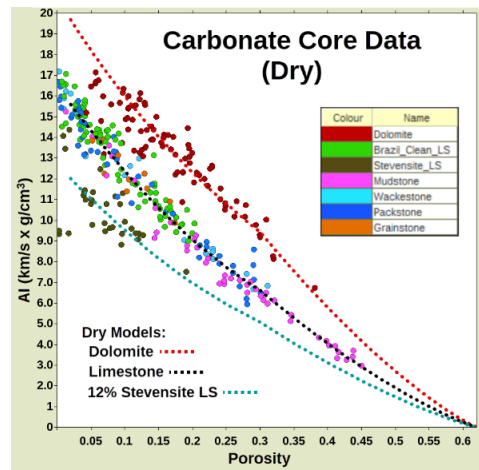

Figure 2: *AI* vs. porosity for the carbonate database with the Vernik-Kachanov RPM lines superposed. Color-code shows different facies and/or geographical affinities.

We present our global sand and shale calibration, fully described in Mur and Vernik (2019), in similar cross-plot domains to demonstrate the flexibility of the model e.g. note the larger impedance reduction with increased porosity past the consolidation porosity point, $\phi_{con} = 0.26$ in Figure 3. As the sandstone dataset was derived from well log data, it was necessary to remove the in situ fluids using a Gassman dry-rock modeling workflow (per-well) and "re-saturate" the samples with common brine properties to reliably calibrate the model. The shale model (calibration also previously described) exhibits a very good fit to the dataset, with only slight drift at very low impedances. We expect that this may simply be due to biases in the flexural mode dispersion correction.
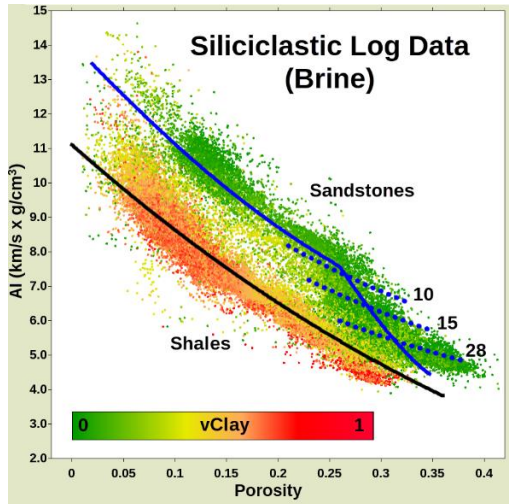
Figure 3: *AI* vs. porosity for the sand and shale database with the RPM lines. Dotted lines represent Mori-Tanaka-Benveniste Poorly Consolidated Sands realized with pore shape factors. Color-code shows clay volume.

Table 1: Elastic properties used in RPM calibration (green) and fluid substitution (blue).

Formation/Fluid	Bulk Modulus (GPa)	Shear Modulus (GPa)	Density (g/cm³)
Limestone	63.7	31.7	2.71
Dolomite	94.9	45.0	2.85
Quartz	37.0	44.0	2.65
Stevensite	11.0	5.0	2.35
Dry Clay	22.1	8.5	2.73
Brine	3.43		1.12
Oil	0.79		0.71
Gas	0.04		0.15

Table 2: The VK RPM model parameters.

Facies	p_{sphere}	q_{sphere}	b_p	b_q	$A(\nu_m)$	$B(\nu_m)$
Limestone	2.51	1.92	16	11	3.83	1.39
Dolomite	2.58	1.91	6	4	3.96	1.38
Arenite	1.79	2.05	14	18	2.72	1.60

For the carbonates, we apply the Gassmann routine to "saturate" both the data and the model with three fluid scenarios (100% brine, 80% oil, and 80% gas) and show the results in Figure 4a using a seismic attribute plot domain (*AI* vs. V_P/V_S) typically used in AVO inversion and reservoir characterization in general. As shown in Figure 4, all brine-saturated rocks from our database tightly plot along the VK model line, which displays significant nonlinearity on the lower impedance end, terminating at the critical porosity, where the rock loses its coherence.

We previously demonstrated that a tight distribution of the dolomites, microporous mudstones and slightly clay-contaminated limestones in the *AI*-V_P/V_S space implies that discriminating among the water-bearing carbonate facies, especially at lower porosities using AVO techniques may be unfeasible. Here we highlight that among the clean carbonates, particularly at high and medium porosities, the fluid substitution results suggest a greater potential for hydrocarbon discrimination. Interestingly, when compared with sands

(Figure 4b), the V_P/V_S contrasts observed in the carbonate fluid cases are similar. Generally, the low frequency (Gassmann's routine) response to hydrocarbon saturation for the majority of medium to low impedance rocks is much more optimistic.
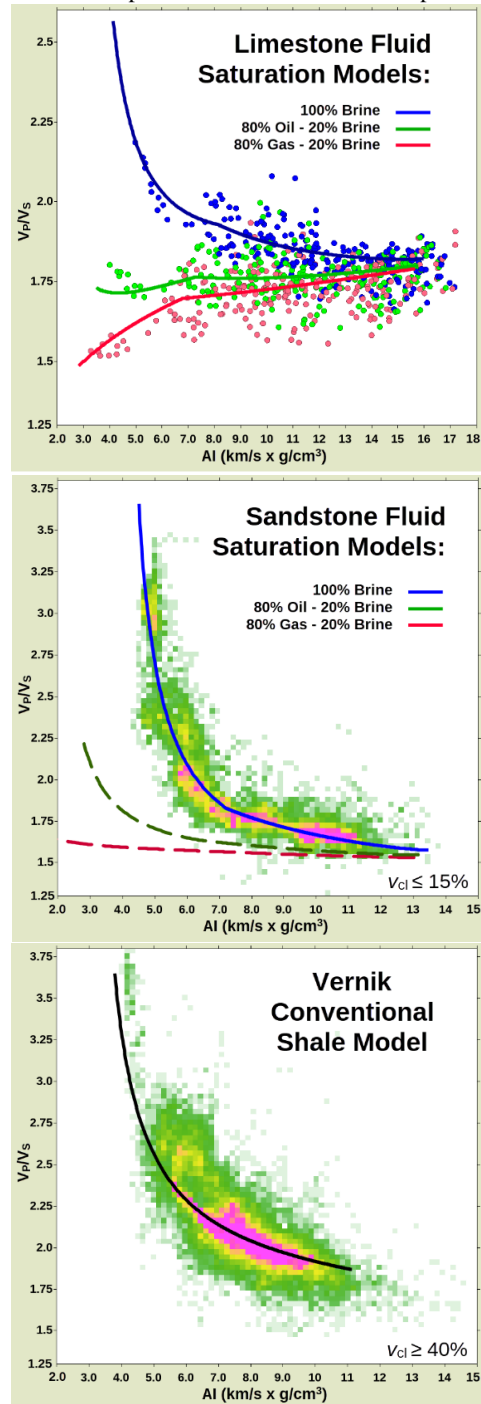

Figure 4: V_P/V_S vs. *AI* plots showing (a) carbonate core sample results of oil (green) and gas (pink) saturation using the Gassmann model with respective RPM lines superposed, (b) brine sand log data (point density) and calibrated RPM with fluid cases, and (c) shale data with calibrated RPM.

SEISMIC AVO MODELING

We apply our calibrated RPM to two key scenarios that represent global challenges in reservoir targeting: (1)

Carbonate pinnacle reef reservoir (Offshore Sarawak or Vietnam analogs) – a shale overburden on a dolomite rich reservoir with varying porosity and gas saturation atop a calcite rich limestone underburden (lithologies based on Sams et al. (2017) and modeled with the calibrated VK models), and (2) Fluvial to shallow-marine sandstone reservoir (Browse Basin, Plover Formation analog) - shales and volcanics overlying a tight sand reservoir sitting on shale and sand interbedded carbonates.

For both sets of AVO models (Figures 5 and 6), we minimize permutations by simplifying the over- and underburden variations, but also acknowledge that the complexity of the neighboring units and inter-reservoir heterogeneity creates further testable scenarios. Reservoir thickness in both presented examples is set to 60m, although additional 2D geometries and interfaces have been modeled. All synthetics were generated with the Zoeppritz (1919) reflectivity model, convolved with a zero phase, SEG-Standard polarity wavelet with dominant frequency of 38 Hz at a range of incident angles. In our first scenario, Browse basin, we chose to model 9% porosity clean arenite reservoir rock (92.5/7.5% mixture Quartz and Dry Clay) with variable fluid fill (100% Brine case and 90%-10% Gas-Brine mix), clay variations from clean sand to wackestone (3% and 15% clay, respectively) and porosity variations of +/- 3%. AVO changes are least sensitive to fluid fill in the lower porosity regions, with the clearest AVO Class IIp effect occurring as porosity increases to 12%. The increased porosity may potentially make reservoir top mapping on full-stack data more difficult. Increased clay content is seen to decrease the AVO gradient at the top of the reservoir, but could also be misinterpreted as higher porosity clean reservoir.

In the pinnacle reef carbonates scenario, we modeled variations in porosity (ϕ=19-39%) and saturation (S_G=0-90%) in the reservoir limestone (grainstone). We observe similar behavior with brine or gas saturation at the 19% and 29% porosity scenarios. However, at higher porosities, the gas case produces Class IIp behavior, implying optimism for a high-grading attribute (high porosity, high gas saturation) using AVO attributes and seismic inversion. Additional scenario testing is necessary to understand other potential false-positive AVO indicators.

DISCUSSION AND CONCLUSIONS

The Vernik-Kachanov RPM has demonstrated specific advantages over the ellipsoidal inclusion-based methods, in which pores are described as ellipsoids with aspect ratios (AR) estimated by pore inscription (Baechle et al., 2008). The approach used in the VK model separates the compliance contribution of pores from that of cracks (microcrack), with the latter having negligible contribution to the total porosity of the rock. In addition, this approach allows the true pore geometries to be evaluated (at least in 2D, Jaeger et al., 2007), which may open the possibility of cross-property mapping, including permeability and irreducible water saturation. The real pore shapes can be imaged using petrographic techniques and their shape factor distributions readily evaluated as shown in Figure 1. The great benefit to this technique is that local geological descriptions and observations can be used to calibrate the model in an unambiguous fashion. The resulting elastic properties from petrophysical perturbations are more likely to be accurate, thus exploration and development objectives can be better realized.
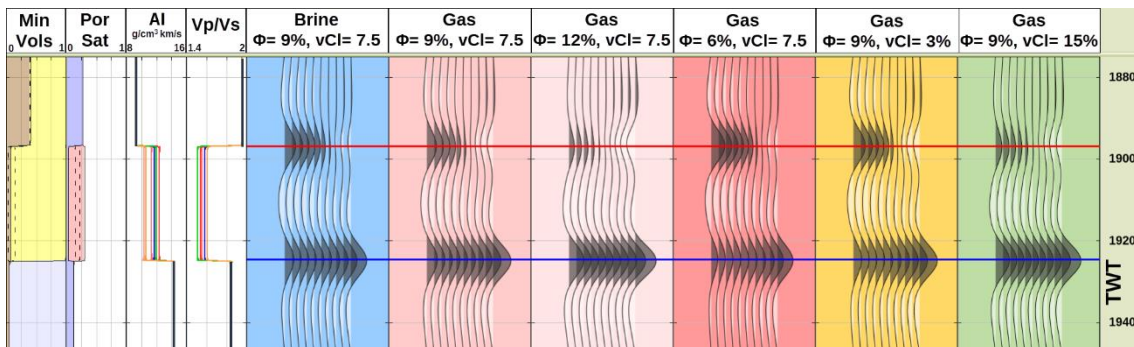

Figure 5: Synthetic gathers derived for the 1st scenario – Browse basin. Reservoir sand with porosity varying from 6-12% and gas saturation varying from 0-90%, and clay content varying from 3 to 15%.
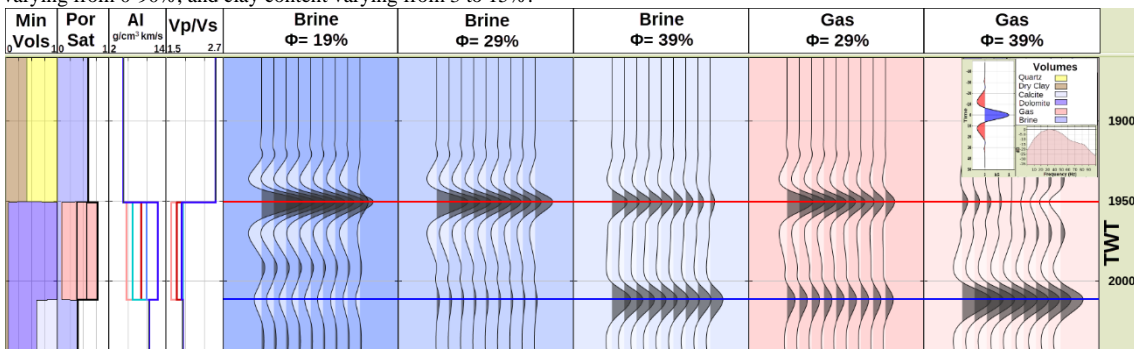

Figure 6: Synthetic gathers derived for the 2nd scenario – Carbonate pinnacle reef. Dolomite rich reservoir at 19, 29 and 39% with 90% gas saturation scenarios at the larger porosity points.

REFERENCES

Baechle, G. T., A. Colpaert, G. P. Eberli, and R. J. Weger. 2008, Effects of microporosity on sonic velocity in carbonate rocks. The Leading Edge, **27**, no. 8,1012-1018. doi: 10.1190/1.2967554.

Cantrell, D. L., and R. M. Hagerty. 1999, Microporosity in arab formation carbonates, Saudi Arabia. GeoArabia, **4**, no. 2,129-154.

Dunham, R. J. 1962, Classification of carbonate rocks according to depositional textures.

Fabricius, I. L., G. T. Bächle, and G. P. Eberli. 2010, Elastic moduli of dry and water-saturated carbonates—Effect of depositional texture, porosity, and permeability. Geophysics, **75**, no. 3,N65-N78.

Jaeger, J. C., N. G. Cook, and R. Zimmerman. 2007, Fundamentals of rock mechanics: John Wiley & Sons.

Kachanov, M. 1993, Elastic solids with many cracks and related problems, Advances in applied mechanics: Elsevier. 259-445.

Mur, A., C. Purcell, Y. Soong, D. Crandall, T. R. McLendon, I. V. Haljasma, R. Warzinski, B. Kutchko, S. Kennedy, and W. Harbert. 2011, Integration of core sample velocity measurements into a 4D seismic survey and analysis of SEM and CT images to obtain pore scale properties. Energy Procedia, **4**,3676-3683.

Mur, A., and L. Vernik. 2019, Testing popular rock-physics models. The Leading Edge, **38**, no. 5,350-357.

Mur, A., and L. Vernik. 2020, Rock physics modeling of carbonates, SEG Technical Program Expanded Abstracts 2020. 2479-2483.

Rafavich, F., C. S. C. Kendall, and T. Todd. 1984, The relationship between acoustic properties and the petrographic character of carbonate rocks. Geophysics, **49**, no. 10,1622-1636.

Sams, M., P. Begg, and T. Manapov. 2017, Seismic inversion of a carbonate buildup: A case study. Interpretation, **5**, no. 4,T641-T652. doi: 10.1190/int-2017-0081.1.

Vasquez, G. F., M. J. Morschbacher, C. W. D. d. Anjos, Y. M. P. Silva, V. Madrucci, and J. C. R. Justen. 2019, Petroacoustics and composition of presalt rocks from Santos Basin. The Leading Edge, **38**, no. 5,342-348. doi: 10.1190/tle38050342.1.

Vernik, L. 2016, Seismic petrophysics in quantitative interpretation: Society of Exploration Geophysicists.

Vernik, L., and M. Kachanov. 2010, Modeling elastic properties of siliciclastic rocks. Geophysics, **75**, no. 6,E171-E182.

Zoeppritz, K. 1919, On the reflection and penetration of seismic waves through unstable layers. Goettinger Nachr, **1**,66-84.